SOURCE
DATA

TRANSPARENT
PROCESS

THE
EMBO
JOURNAL

SCA8 RAN polySer protein preferentially accumulates in white matter regions and is regulated by eIF3F

Fatma Ayhan[1,2,†], Barbara A Perez[1,2,†], Hannah K Shorrock[1,2], Tao Zu[1,2], Monica Banez-Coronel[1,2], Tammy Reid[1,2], Hirokazu Furuya[3,4], H Brent Clark[5], Juan C Troncoso[6], Christopher A Ross[7,8,9,10,11], SH Subramony[1,12], Tetsuo Ashizawa[13], Eric T Wang[1,2], Anthony T Yachnis[14] & Laura PW Ranum[1,2,12,15,*] [iD]

Abstract

Spinocerebellar ataxia type 8 (SCA8) is caused by a bidirectionally transcribed CTG·CAG expansion that results in the *in vivo* accumulation of CUG RNA foci, an ATG-initiated polyGln and a polyAla protein expressed by repeat-associated non-ATG (RAN) translation. Although RAN proteins have been reported in a growing number of diseases, the mechanisms and role of RAN translation in disease are poorly understood. We report a novel toxic SCA8 polySer protein which accumulates in white matter (WM) regions as aggregates that increase with age and disease severity. WM regions with polySer aggregates show demyelination and axonal degeneration in SCA8 human and mouse brains. Additionally, knockdown of the eukaryotic translation initiation factor eIF3F in cells reduces steady-state levels of SCA8 polySer and other RAN proteins. Taken together, these data show polySer and WM abnormalities contribute to SCA8 and identify eIF3F as a novel modulator of RAN protein accumulation.

Introduction

Spinocerebellar ataxia type 8 (SCA8) is a dominantly inherited neurodegenerative disease caused by a CTG·CAG microsatellite expansion mutation (Koob *et al*, 1999; Moseley *et al*, 2006). SCA8 most frequently presents as an adult-onset disease characterized by limb and gait ataxia, dysarthria, and nystagmus (Day *et al*, 2000; Zeman *et al*, 2004), but infantile- and juvenile-onset cases and cases with cognitive and psychiatric symptoms have also been reported (Felling & Barron, 2005; Lilja *et al*, 2005). The SCA8 mutation is bidirectionally expressed producing both CAG (*ATXN8*) and CUG (*ATXN8OS*) expansion transcripts (Moseley *et al*, 2006). Both transcripts are thought to contribute to disease by RNA and protein gain-of-function (GOF) mechanisms. CUG expansion transcripts form RNA foci that sequester MBNL proteins leading to RNA GOF effects (Daughters *et al*, 2009). In addition, SCA8 CAG expansion transcripts have been shown to result in the expression and accumulation of an ATG-initiated polyglutamine expansion protein and a repeat-associated non-ATG (RAN) polyalanine expansion protein in brains of SCA8 BAC mice and SCA8 autopsy tissue (Moseley *et al*, 2006; Zu *et al*, 2011).

RAN translation has been shown to occur in seven different repeat expansion diseases (SCA8, SCA31, DM1, DM2, HD, FXTAS, and ALS/FTD; Zu *et al*, 2011, 2013, 2017; Ash *et al*, 2013; Mori

1   Center for NeuroGenetics, College of Medicine, University of Florida, Gainesville, FL, USA
2   Department of Molecular Genetics and Microbiology, College of Medicine, University of Florida, Gainesville, FL, USA
3   Department of Neurology, Kochi Medical School, Kochi University, Kochi, Japan
4   Department of Neurology, Neuro-Muscular Center, NHO Omuta Hospital, Fukuoka, Japan
5   Department of Laboratory Medicine and Pathology, University of Minnesota Medical School, Minneapolis, MN, USA
6   Department of Pathology and Neurology, The Johns Hopkins University School of Medicine, Baltimore, MD, USA
7   Department of Psychiatry, The Johns Hopkins University School of Medicine, Baltimore, MD, USA
8   Department of Neurology, The Johns Hopkins University School of Medicine, Baltimore, MD, USA
9   Department of Pharmacology, The Johns Hopkins University School of Medicine, Baltimore, MD, USA
10 Department of Neuroscience, The Johns Hopkins University School of Medicine, Baltimore, MD, USA
11 Huntington's Disease Center, The Johns Hopkins University School of Medicine, Baltimore, MD, USA
12 Department of Neurology, College of Medicine, University of Florida, Gainesville, FL, USA
13 Department of Neurology, Houston Methodist Hospital, Houston, TX, USA
14 Department of Pathology, Immunology and Laboratory Medicine, College of Medicine, University of Florida, Gainesville, FL, USA
15 Genetics Institute, University of Florida, Gainesville, FL, USA
    *Corresponding author. Tel: +1 352 294 5209; E-mail: ranum@ufl.edu
    † These authors contributed equally to this work

et al, 2013; Todd *et al*, 2013; Bañez-Coronel *et al*, 2015; Ishiguro *et al*, 2017). While the demonstration that sense and antisense RAN proteins accumulate in a growing number of diseases suggests they contribute to these disorders, the pathogenic consequences of RAN proteins are not yet clear. Understanding the common themes of RAN translation across multiple disorders will provide insight into the molecular mechanisms of these disorders.

Here, we report a novel toxic SCA8 RAN polySer protein that accumulates in SCA8 patient autopsy tissue and SCA8 BAC transgenic mice. This SCA8 RAN polySer protein accumulates in white matter regions that show demyelination and axonal degeneration. The preferential white matter distribution of the SCA8 RAN polySer protein and elevated expression of eIF3F in white matter regions led to the identification of eIF3F as a mammalian translation initiation factor able to regulate RAN protein levels *in vitro*. In summary, these data suggest a model in which a novel RAN polySer protein causes white matter abnormalities that contribute to SCA8 and demonstrate that RAN protein levels can be modulated independent of AUG-initiated proteins.

Results

ATXN8 transcript is expressed at a higher level than *ATXN8OS* in SCA8 mice cerebellum

To explore the relative contribution of the *ATXN8* and *ATXN8OS* transcripts in SCA8, we measured the relative abundance of these transcripts in cerebellum from SCA8 BAC transgenic mice. SCA8 mice express the full-length human *ATXN8* and *ATXN8OS* genes from a BAC transgene that includes flanking regions to allow for the endogenous spatiotemporal expression patterns of the transgenes (Moseley *et al*, 2006). RNA sequencing reads of *ATXN8* and *ATXN8OS* transcripts were mapped back to a region of the human reference genome containing *ATXN8* and *ATXN8OS* plus 10 kb of upstream and downstream flanking sequence. *ATXN8OS* expression was calculated based on the number of reads that map to exons B, C, and D which do not overlap the *ATXN8* sequence. Reads in the last intron of *ATXN8OS* which overlaps *ATXN8* were used to differentiate the two transcripts and to calculate the relative levels of *ATXN8* (Fig 1A). These data show that *ATXN8* transcripts are expressed ~7.5-fold higher than *ATXN8OS* transcripts in SCA8 mouse cerebellum ($P < 0.0001$; Fig 1B).

Novel polySer RAN proteins accumulate in SCA8 human and mouse brain

Because *ATXN8* transcripts are expressed at higher levels than *ATXN8OS*, and at levels sufficient for the accumulation of AUG-initiated polyGln (M-polyGln; Moseley *et al*, 2006) and RAN polyAla expansion proteins (Zu *et al*, 2011), we developed antibodies to test the hypothesis that RAN polySer proteins accumulate in SCA8 and contribute to disease. RAN translation of the *ATXN8* expansion in the AGC frame is predicted to produce a polySer RAN protein followed by a unique 42 amino acid C-terminal region (Figs 1C and EV1A). We generated two rabbit polyclonal antibodies, α-SerCT and α-SerCT2, directed at different non-overlapping peptide sequences within the unique C-terminal region downstream of the predicted

SCA8 polySer protein (Fig EV1A). The specificity of the antibodies was validated by immunofluorescence (IF) and protein blots of transfected cells expressing epitope-tagged polySer with the predicted C-terminal sequence (Fig EV1B and C).

Next, we tested whether the predicted polySer RAN proteins could be detected *in vivo* by immunohistochemistry (IHC). We found robust positive staining in both SCA8 mouse and human autopsy tissue. Although both α-SerCT antibodies showed similar punctate staining, α-SerCT was used for IHC analyses of SCA8 BAC mouse tissue as it showed less background reactivity. In SCA8 BAC mice, we detected widespread punctate aggregates of variable size in brain regions primarily affected in the disease, including the cerebellum and brainstem (Fig 1D). In addition to hindbrain regions, robust protein accumulation is found throughout layers II and III of the cerebral cortex, the dentate gyrus, and CA regions of the hippocampus and the midbrain (e.g., Fig 1D and E). Aggregates can show perinuclear localization or punctate staining throughout the brain regions. No similar staining is found in age-matched non-transgenic (NT) control animals (Fig 1D and E) or in SCA8 animals with preimmune serum (Fig EV1D).

Both antibodies were also able to detect polySer aggregates in patient autopsy tissue. However, because α-SerCT2 showed less non-specific reactivity in human tissue, α-SerCT2 was used for subsequent IHC on human tissue (Fig EV1E). Examination of seven SCA8 human autopsy cases shows similar aggregates in the cerebellum, brainstem, and cortex but not in unaffected or disease controls (Fig 1F, Table 1).

Taken together, these data demonstrate that *ATXN8* transcripts express a novel homopolymeric polySer RAN protein which accumulates as aggregates in multiple brain regions in SCA8 mice and human autopsy tissue.

RAN PolySer and M-polyGln proteins show distinct patterns of accumulation

To better understand SCA8 pathology, we compared the distribution of the polySer RAN protein with the previously characterized AUG-initiated M-polyGln expansion protein. Although both proteins are expressed from *ATXN8* transcripts, their distribution patterns in the cerebellum are strikingly different. IHC performed on serial cerebellar sections shows polyGln, but not RAN polySer aggregates accumulate in Purkinje cell nuclei. In contrast, we detected polySer but not polyGln aggregates in the molecular layer and oligodendrocyte-rich subcortical and deep cerebellar white matter regions (Fig 2A). In the cortex, hippocampus, and brainstem, polyGln and polySer aggregates are often found in close proximity; however, they are detected as discrete aggregates. Double-labeling of polyGln and RAN polySer by IF shows no overlap in signal in the frontal cortex, brainstem (pons), or hippocampus. These data suggest that polySer and polyGln aggregates are found in different cells or different cellular compartments in these brain regions. PolyGln staining in these regions is primarily nuclear. In contrast, polySer aggregates show a perinuclear localization (Fig 2B). Double-labeling experiments show polyGln inclusions are primarily found in NeuN-positive neurons, while the majority of polySer aggregates do not co-localize with NeuN-positive neurons (Fig 2C). To further clarify the cellular localization of RAN polySer, we performed double-labeling IF of polySer and CNPase, a marker of oligodendrocytes, and show that polySer
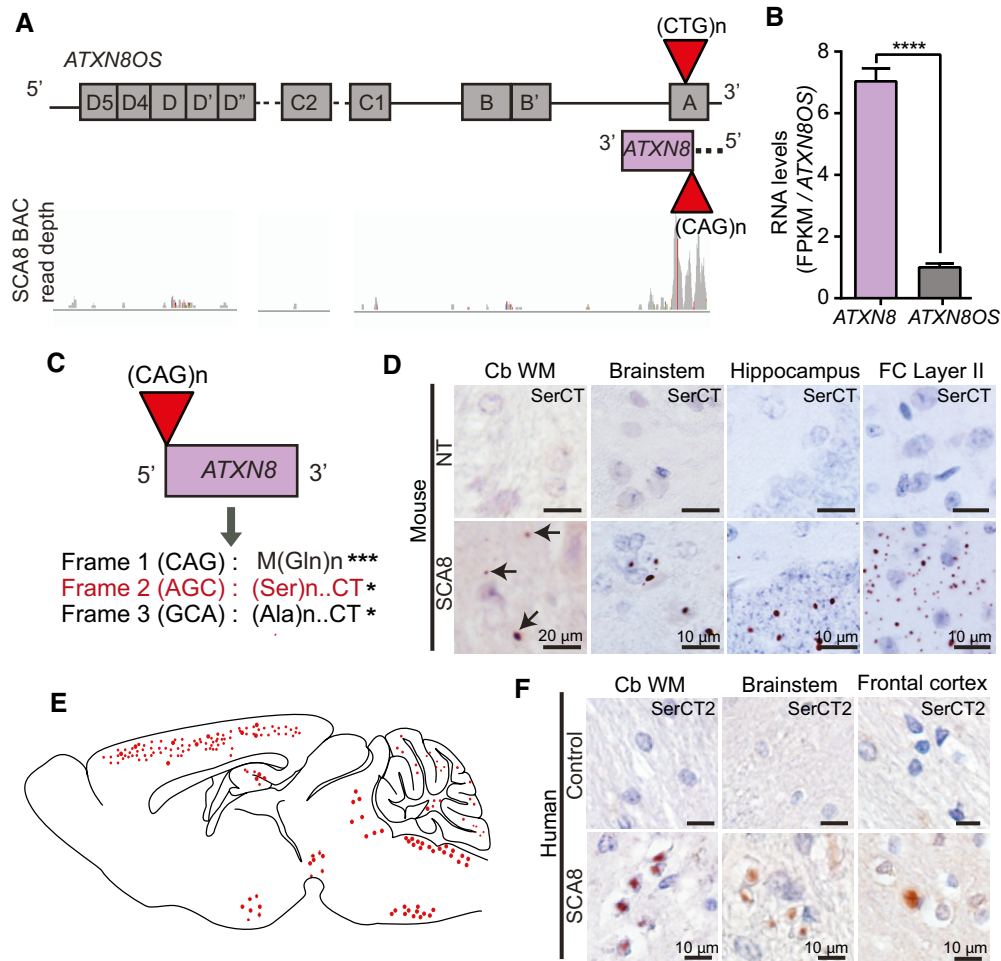
Figure 1. Novel polySer RAN protein encoded by the higher expressing *ATXN8* transcript in SCA8.

A Schematic diagram of *ATXN8OS* (top strand) and *ATXN8* (bottom strand). RNA-Seq read coverage visualized by Integrative Genomic Viewer across the *ATXN8/ATXN8OS* locus is depicted.

B Bar graph showing relative mRNA levels of *ATXN8* and *ATXN8OS*. FPKM values for each transcript are normalized to FPKM value for *ATXN8OS*. (****$P < 0.0001$; mean $\pm$ SEM; unpaired t-test) FPKM, fragments per kilo base of transcript per million mapped reads.

C Known and predicted homopolymeric protein expressed across SCA8 CAG expansion (*ATXN8*) transcripts. * Represent stop codons.

D Immunohistochemistry of 10- to 12-month-old end-stage SCA8 BAC mice brain tissue shows accumulation of novel polySer RAN protein (detected by unique antibody to the polySer protein C terminus, α-SerCT) in cerebellar white matter, brainstem, hippocampus, and layer II of the frontal cortex. Representative polySer aggregates are indicated by black arrows. No aggregates are found in age-matched non-transgenic (NT) littermates ($n = 6$ for each cohort).

E Schematic of a sagittal section of mouse brain shows the distribution of polySer RAN protein in SCA8 BAC expansion mice. Red circles represent variable size and frequency of polySer aggregates throughout different brain regions.

F Immunohistochemistry of human SCA8 autopsy tissue ($n = 4$–7) shows accumulation of novel polySer RAN protein in cerebellar white matter, brainstem, and frontal cortex.

aggregates located in the white matter are close to or within oligo-dendrocytes/myelinated axons (Fig EV2). Similarly, in humans SCA8 polySer and polyGln proteins accumulate in distinct cerebellar regions, with polySer found primarily in the deep cerebellar white matter and polyGln in Purkinje cell nuclei (Fig 2D). Despite this, there are some differences in the appearance of polySer in human post-mortem tissue and SCA8 BAC mouse brain. These differences may be due to the end stage of disease in the human cases and to differences in tissue handling and processing including post-mortem delay and the severity of disease at endpoint in human cases.

In summary, SCA8 polySer and polyGln proteins, which are expressed from alternative reading frames of the *ATXN8* transcripts, show strikingly distinct patterns of accumulation. These data suggest cell-specific factors that affect reading frame selection or protein turnover may lead to differences in the regional and cellular accumulation patterns of these proteins.

SCA8 polySer aggregates increase with age and disease progression

The SCA8 BAC mice begin to show severe neurological phenotypes at 4 months of age including marked rotarod deficits and hindlimb stiffness. These phenotypes progressively worsen to include inactivity, generalized wasting, kyphosis, priapism resulting in premature death at ~6 months of age (Moseley *et al*, 2006). To better model the late stages of SCA8 in our mice, we provided supportive care,

Table 1. Summary of polySer staining in SCA8 and control autopsy tissue.

Case		Age	Sex	SCA8 Repeat	PMI	Cerebellum	Brainstem	Frontal Cortex
SCA8	1	80	F	104	28	+++	++	+
	2	74	F	109	11.5	+++	+	+
	3	85	F	91	8	++	+	n.d
	4	76	M	197	4.5	+	n.d	+
	5	83	M		7	+++	++	−
	6	59	F	790		+++	n.d	+
	7	60	F	105	10	+++	n.d	n.d
CTRL	1					n.d	n.d	−
	2					n.d	n.d	−
	3	40	M		6	−	−	−
	4	45	F		20	−	−	n.d
HD	1	46	F		7	−	−	
HDL2	1	41	F		3	−	−	−
SCA2	1	56	F		3.5	−	n.d	n.d
SCA5	1		M			−	−	n.d
SCA7	1	59	F		22	−	n.d	n.d
DM1	1	68	F			−	−	−

RAN staining: −, negative; +, low-intensity staining; ++, moderate intensity; +++, frequent and intense; ++++, highly frequent positive cells with high-intensity staining. SCA8, spinocerebellar ataxia type 8; CTRL, control; HD, Huntington disease; HDL2, Huntington disease like-2; SCA2, spinocerebellar ataxia type 2; SCA5, spinocerebellar ataxia type 5; SCA7, spinocerebellar ataxia type 7; DM1, myotonic dystrophy type 1; n.d, not determined; M, male; F, female; PMI, post-mortem interval.

including an accessible gel-diet and water source. These simple changes substantially extended the life span of the mice to ~10–12 months of age.

We performed IHC at different ages to address how polySer RAN protein aggregates change over time and disease progression (Fig 3A). To do this, we identified regions that showed polySer aggregates at 2 months of age and quantified the number of polySer aggregates in these regions at 2, 6, and 10 months of age. At 2 months, when SCA8 animals show no overt cage behavior phenotypes, IHC showed very small, pin-like polySer aggregates that were found infrequently in brainstem regions including the vestibular nuclei and cuneate nuclei but not detectable in the cerebellum or hippocampus. At 6 months of age, when marked phenotypes are apparent and would be fatal without supportive care, the size and the number of polySer RAN aggregates in the brainstem substantially increase and small aggregates are now apparent throughout the frontal cortex. At ~10 months of age, when animals show advanced end-stage disease, polySer aggregates were larger in size and more abundant in both the brainstem and frontal cortex. Quantification of polySer aggregates in the motor cortex and brainstem (vestibular nucleus and cuneate nucleus) showed an increase in aggregates from 2–10 and 6–10 months of age (Fig 3A).

Although there were no overt cage behavior abnormalities at 2 months of age, small punctate polySer aggregates were detected in the vestibular and cuneate nuclei of the brainstem. Because these nuclei are associated with proprioception and gait, we examined 2-month-old SCA8 mice for early signs of disease using open field and DigiGait tests. Open field analysis showed decreased ambulatory distance and time and increased resting time in 2-month SCA8

mice compared to age-matched NT controls (Fig 3B). Additionally, SCA8 animals showed significant differences in 13 DigiGait parameters including abnormal gait symmetry and decreased propulsion time (Table 2). Although motor abnormalities can be associated with muscle pathology, previous reports did not detect expression of *ATXN8* or *ATXN8OS* transcripts in muscle of SCA8 BAC mice (Moseley *et al*, 2006), suggesting that these phenotypes are due to CNS features of the disease.

In summary, polySer aggregates increase with age and disease progression in SCA8 mice. Initial sites of polySer accumulation in the brainstem of 2-month-old mice are consistent with the early motor abnormalities found in these animals.

RAN polySer-positive white matter regions show degenerative phenotypes

Previously, we focused our neuropathological assessment of the SCA8 BAC mice on the cerebellar Purkinje cell, granule cell, and molecular layers, which all appeared relatively normal (Moseley *et al*, 2006). Our detection of polySer in white matter regions of the brain led us to more thoroughly examine white matter regions in SCA8 for neuropathological changes. H&E staining of cerebellar sections from severely affected SCA8 mice showed widespread vacuolization of the subcortical and deep cerebellar white matter regions compared to NT controls (Fig 4A). Because vacuolization can be caused by lipid loss during ethanol dehydration (Wells & Wells, 1989), this observation suggested the possibility that the SCA8 mice have underlying white matter pathology that makes it more sensitive to vacuole formation (Kuwamura *et al*, 2002;
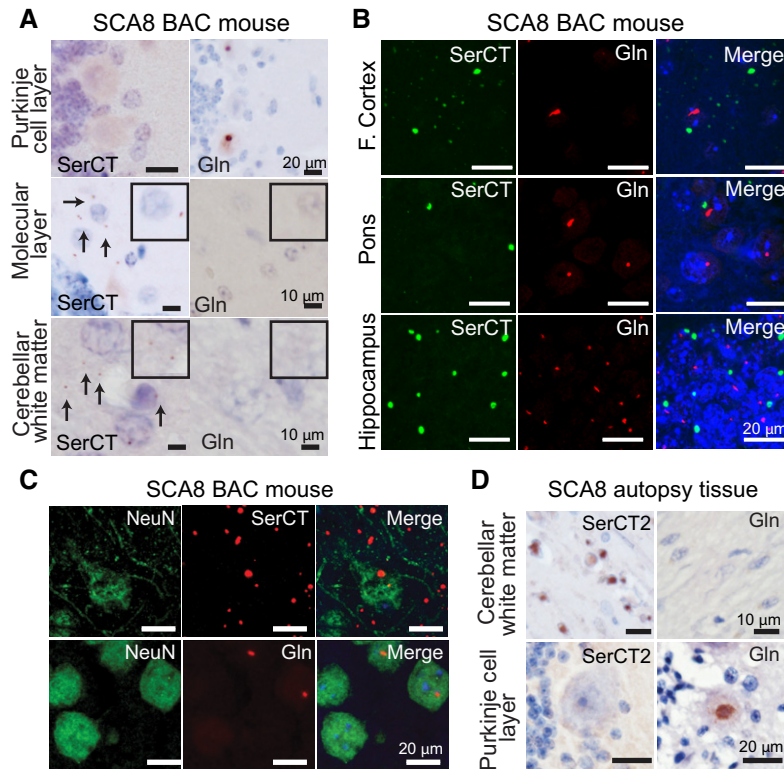
Figure 2. Distribution differences of polySer and polyGln proteins in SCA8 BAC mouse and human autopsy brains.

A Immunohistochemistry (IHC) of end-stage SCA8 BAC mouse cerebellum shows that polySer but not polyGln is found in the molecular layer and cerebellar white matter and that polyGln but not polySer accumulates in Purkinje cells. Representative polySer aggregates are indicated by black arrows. Inset: higher magnification of molecular layer and white matter.

B IF double staining shows no co-localization of polyGln and polySer in frontal cortex, pons, or hippocampus of end-stage SCA8 BAC mice.

C IF double staining of end-stage SCA8 BAC frontal cortex shows exclusive localization of polyGln (mouse α-Gln, red, bottom panel) in neurons (rabbit α-NeuN, green, bottom panel). In contrast, polySer (Rabbit α-SerCT, red, top panel) shows widespread accumulation in the frontal cortex including within neurons (mouse α-NeuN, green, top panel).

D IHC of SCA8 human cerebellum shows that polySer accumulates in the white matter but not in the Purkinje cells (left panels), while polyGln accumulates in Purkinje cells but not cerebellar white matter (right panels).

Garman, 2011; Cognat *et al*, 2014). To test white matter integrity in SCA8, we examined serial cerebellum and brainstem sections for demyelination and axonal degeneration in the polySer-positive regions. Luxol fast blue (LFB) staining shows demyelination in both the cerebellum and brainstem from SCA8 mice compared to NT controls. Additionally, IHC using an antibody against total neurofilament H (SMI-32) shows evidence of axonal degeneration (Fig 4A).

Similar changes were found in human autopsy tissue, with evidence for demyelination and axonal degeneration in deep cerebellar white matter (Fig 4B). These sites of white matter pathology are positive for RAN polySer, but not for polyGln (Fig 4B) and are consistent with white matter abnormalities previously found by imaging and neuropathology in SCA8 patients (Kumar & Miller, 2008; Kim *et al*, 2013; Yokoyama *et al*, 2014). In contrast, brain regions that did not show polySer aggregates in SCA8 BAC mouse cerebellum (Fig EV3A) and human cortical white matter (Fig EV3B) did not show evidence of demyelination.

To further characterize the oligodendrocyte abnormalities in the polySer-positive white matter regions, we performed IHC using a cytoplasmic marker of mature oligodendrocytes (CC1) in SCA8 mice. Consistent with the demyelination shown above, these data

show a decreased number of mature oligodendrocytes in the deep cerebellar white matter regions of SCA8 animals compared to controls (Fig 4C).

Additionally, GFAP staining of the deep cerebellar white matter regions shows evidence for reactive astrogliosis in SCA8 compared to NT animals with a 50% increase in relative GFAP staining (Fig 4D). Reactive astrogliosis has been implicated in a wide range of neurodegenerative diseases and is often observed in demyelinated lesions within white matter (Schmahmann *et al*, 2008).

Because we observed degenerative phenotypes in white matter regions where polySer, but not polyGln, aggregates are found, we next tested the cellular toxicity of SCA8 polyGln and polySer expansion proteins independent of each other using ATG-initiated codon replacement constructs: ATG-Alt-Gln and ATG-Alt-Ser. We generated alternative codon constructs by selecting different nucleotide sequences that encode the same polyGln or polySer expansion proteins but are unable to form the RAN-permissive hairpin structure (Zu *et al*, 2011) and, instead, only express ATG-initiated polyGln or polySer expansion proteins. These alternative codon, non-hairpin forming transcripts allow us to study the toxic effects of individual homopolymeric proteins independent of CAG RNA
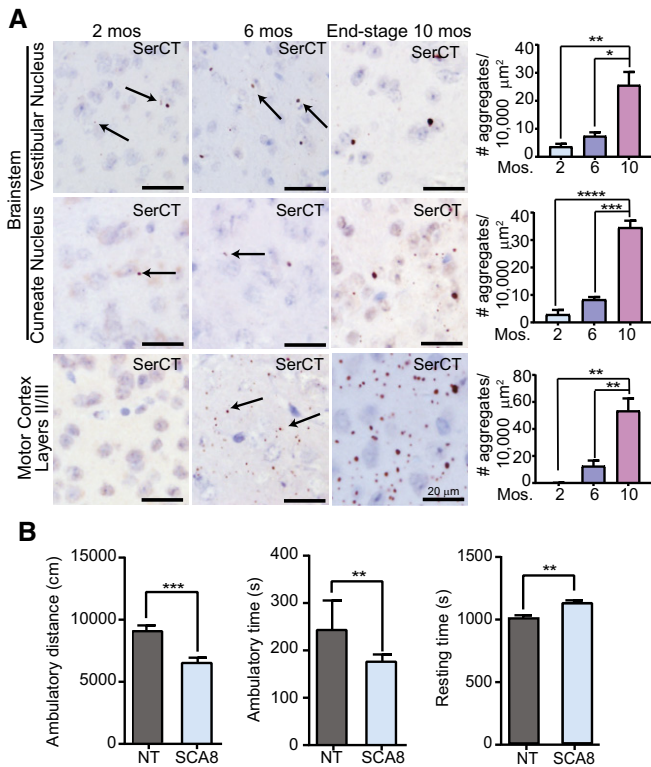
Figure 3. PolySer accumulation increases with age and severity of disease.

A   Representative images of the vestibular nucleus (upper panels), cuneate nucleus (middle panels), and motor cortex layers II/III (lower panels) of SCA8 BAC mice at 2 months (left panels), 6 months (middle panels), and end-stage (10 months, right panels) stained with α-SerCT. Representative aggregates are indicated by black arrows. Corresponding quantifications of polySer aggregates for each region on the right ($n = 3$; mean ± SEM; one-way ANOVA with Tukey's *post hoc* test; *$P < 0.025$, **$P < 0.005$, ***$P < 0.0005$, ****$P < 0.0001$)

B   Open field analysis of 2-month-old animals shows a significant decrease in ambulatory distance (cm) and ambulatory time (s) and a significant increase in resting time (s) (NT $n = 19$, SCA8 BAC $n = 23$, **$P < 0.01$, ***$P < 0.001$; mean ± SEM; unpaired *t*-test).

gain-of-function effects and effects of other RAN proteins (Bañez-Coronel *et al*, 2015). The ATG-Alt-Ser construct includes an ATG-initiation codon, 107 serine-encoding codons (TCT-TCC), and the unique C-terminal region after the repeat tract. Similarly, the ATG-Alt-Gln construct has an ATG-initiation codon followed by 107 glutamine-encoding repeats (CAA) and is followed by multiple stop codons mimicking the endogenous mutant SCA8 polyGln protein. It has previously been shown that alternative codon constructs used to encode polyGln and polySer produce polyGln and polySer proteins, respectively (Bañez-Coronel *et al*, 2015).

After demonstrating that the ATG-Alt-Gln and ATG-Alt-Ser constructs express comparable levels of RNA (Fig EV4A), we measured relative levels of cell death using the lactate dehydrogenase (LDH) assay (Korzeniewski & Callewaert, 1983). LDH is a cytoplasmic enzyme, and its release into the media is an indicator of lost membrane integrity and cell death. T98 glial cells expressing polyGln or polySer showed significant increases in cell death

compared to empty vector ($P < 0.00025$). Interestingly, T98 cells expressing polySer showed increased cell death compared to cells expressing polyGln ($P < 0.0025$; Fig 4E).

Taken together, these data show that RAN polySer-positive white matter regions in SCA8 mice have demyelination, axonal degeneration, oligodendrocyte loss, and astrogliosis. Furthermore, *in vitro* studies show polySer expansion proteins are toxic to glial cells independent of the CAG expansion transcripts.

RAN protein levels decreased by knockdown of eIF3F

The accumulation of the SCA8 polySer RAN protein and previously reported HD and DM2 RAN proteins (Bañez-Coronel *et al*, 2015; Zu *et al*, 2017) in white matter regions suggests that RAN translation may be more efficient in specific cell types or brain regions. This raises the possibility that cells within white matter regions express one or more factors that favor RAN translation. RAN-transactivating factors (RAN-TAFs) could function like IRES trans-acting factors (ITAFs) that facilitate translation from IRES sequences (Holcik & Sonenberg, 2005).

The eukaryotic translation factor, eIF3F, was of interest to us as a possible RAN-TAF because the full-length transcript isoform (ENST00000309828.4) was reported to be elevated in white matter compared to gray matter brain regions (Mills *et al*, 2013). It has also been shown that increased levels of eIF3F can downregulate canonical translation (Shi *et al*, 2006) and that eIF3F binds structured IRES sequences (Zhou *et al*, 2008) similar to those that undergo RAN translation. To investigate whether Eif3f expression is higher in white matter than in gray matter, we performed qRT–PCR comparing tease-separated cerebellar white and gray matter from SCA8 BAC mice. To confirm an enrichment of oligodendrocytes in white matter samples, myelin basic protein (MBP) was measured by qRT–PCR. After confirmation of MBP white matter enrichment (Fig EV5A), we performed qRT–PCR and show Eif3f transcripts have a twofold increase in SCA8 BAC cerebellar white matter compared to gray matter (Fig 5A). We also evaluated levels of *ATXN8* RNA in cerebellar gray and white matter and found no significant difference in the expression of ATXN8 transcripts (Fig EV5B), indicating that changes in ATXN8 RNA expression are unlikely to contribute to the increased polySer aggregate accumulation in white matter regions. The elevated *Eif3f* levels observed in cerebellar white matter, which shows robust polySer aggregation, are consistent with the possibility that *eIF3F* increases RAN translation leading to the accumulation of RAN polySer protein in white matter.

To explore the possible role of eIF3F as a RAN-TAF, we tested the effects of eIF3F knockdown on protein accumulation in HEK293T cells expressing expansion proteins with or without an ATG-initiation codon (Fig 5B). First, we tested the effects of eIF3F knockdown on polySer protein accumulation using minigenes with or without an ATG-initiation codon in the polySer frame. siRNA knockdown of eIF3F decreased steady-state levels of RAN polySer proteins expressed from CAG constructs that do not contain an ATG-initiation codon in the polySer frame. PolySer from the A8 and CAG constructs were reduced by 53% ($P < 0.05$) and 66% ($P < 0.01$), respectively. In contrast, eIF3F knockdown did not affect polySer levels in cells transfected with the DM1-3T construct, which contains an ATG-initiation codon in the polySer frame (Fig 5C and D).

Table 2. Gait parameters from DigiGait in SCA8 BAC (forelimb only unless noted) are indicated along with corresponding *P*-value.

Parameters (38 in total)	Units	NT Average ± SEM	SCA8 Average ± SEM	NT vs. SCA8 difference	SCA8 BAC Tg vs. NT
# Parameters P ≤ 0.05					13
# Parameters P < 0.01					3
# Parameters P ≤ 0.05 in forelimb & hindlimb					2
Swing	(s)	0.086 ± 0.002	0.083 ± 0.001	−0.00	ns
Swing/Stride	(%)	36.227 ± 0.392	36.650 ± 0.370	+0.42	ns
Brake	(s)	0.058 ± 0.002	0.050 ± 0.002	+0.00	ns
Brake/Stride	(%)	24.415 ± 0.600	26.366 ± 0.720	+1.95	↑*
Propel	(s)	0.093 ± 0.002	0.083 ± 0.002	−0.01	↓*** Fore; * Hind
Propel/Stride	(%)	39.346 ± 0.703	36.984 ± 0.750	−2.36	↓*
Stance	(s)	0.151 ± 0.002	0.143 ± 0.002	−0.01	↓*
Stance/Stride	(%)	63.773 ± 0.392	63.350 ± 0.370	−0.42	ns
Stride	(s)	0.237 ± 0.004	0.225 ± 0.003	−0.01	↓*
Brake/Stance	(%)	38.323 ± 0.948	41.631 ± 1.120	+3.31	↑*
Propel/Stance	(%)	61.677 ± 0.948	58.369 ± 1.120	−3.31	↓*
Stance/Swing	(real#)	1.773 ± 0.030	1.734 ± 0.027	−0.04	ns
Stride Length	(cm)	5.200 ± 0.084	4.956 ± 0.068	−0.24	↓*
Stride Frequency	(steps/s)	4.346 ± 0.073	4.578 ± 0.068	+0.23	↑*
Paw Angle	(deg)	0.758 ± 1.878	−0.156 ± 1.626	−0.91	ns
Absolute Paw Angle	(deg)	8.950 ± 0.684	8.700 ± 0.527	−0.25	ns
Paw Angle Variability	(deg)	4.715 ± 0.307	5.381 ± 0.202	+0.67	ns
Stance Width	(cm)	1.308 ± 0.040	1.394 ± 0.038	+0.09	ns
Step Angle	(deg)	63.231 ± 1.635	60.081 ± 2.653	−3.15	ns
Stride Length Variability	(cm)	1.011 ± 0.043	1.147 ± 0.048	+0.14	↑*
Stance Width Variability	(cm)	0.442 ± 0.027	0.510 ± 0.036	+0.07	ns
Step Angle Variability	(deg)	17.796 ± 1.393	19.978 ± 1.776	+2.18	ns
# Steps	(real #)	20.154 ± 0.710	21.750 ± 0.980	+1.60	ns
Stride Length CV	(CV %)	19.522 ± 0.894	23.311 ± 1.081	+3.79	↑**
Stance Width CV	(CV %)	33.938 ± 2.440	36.279 ± 2.295	+2.34	ns
Step Angle CV	(CV %)	28.923 ± 2.743	35.864 ± 3.804	+6.94	ns
Swing Duration CV	(CV %)	19.604 ± 0.829	21.488 ± 1.265	+1.84	ns
Paw Area at Peak Stance	(cm^2)	0.185 ± 0.006	0.193 ± 0.005	+0.01	ns
Paw Area Variability at Peak Stance	(cm^2)	0.020 ± 0.002	0.023 ± 0.002	0.00	ns
Stance Factor	(real #)	0.995 ± 0.014	1.003 ± 0.019	+0.01	ns
Gait Symmetry	(real #)	1.002 ± 0.004	1.024 ± 0.006	+0.02	↓** Fore; ** Hind
MAX dA/dT	(cm^2/s)	11.722 ± 0.400	12.144 ± 0.334	+0.42	ns
MIN dA/dT	(cm^2/s)	−3.065 ± 0.094	−3.223 ± 0.130	−0.16	ns
Overlap Distance	(cm)	−0.072 ± 0.290	−0.243 ± 0.360	−0.17	ns
Paw Placement Positioning	(cm)	0.033 ± 0.067	0.098 ± 0.070	+0.06	ns
Ataxia Coefficient	(real #)	0.734 ± 0.042	0.900 ± 0.046	+0.17	↑*
Midline Distance	(cm)	−1.786 ± 0.048	−1.724 ± 0.049	+0.06	ns
Axis Distance	(cm)	0.023 ± 0.129	0.010 ± 0.120	−0.01	ns

#, number; ↑, upregulated; ↓, downregulated; CV, coefficient of variation; ns, *P* ≥ 0.05; *P ≤ 0.05; **P ≤ 0.01; ***P ≤ 0.001; NT *n* = 13; SCA8 BAC *n* = 16.
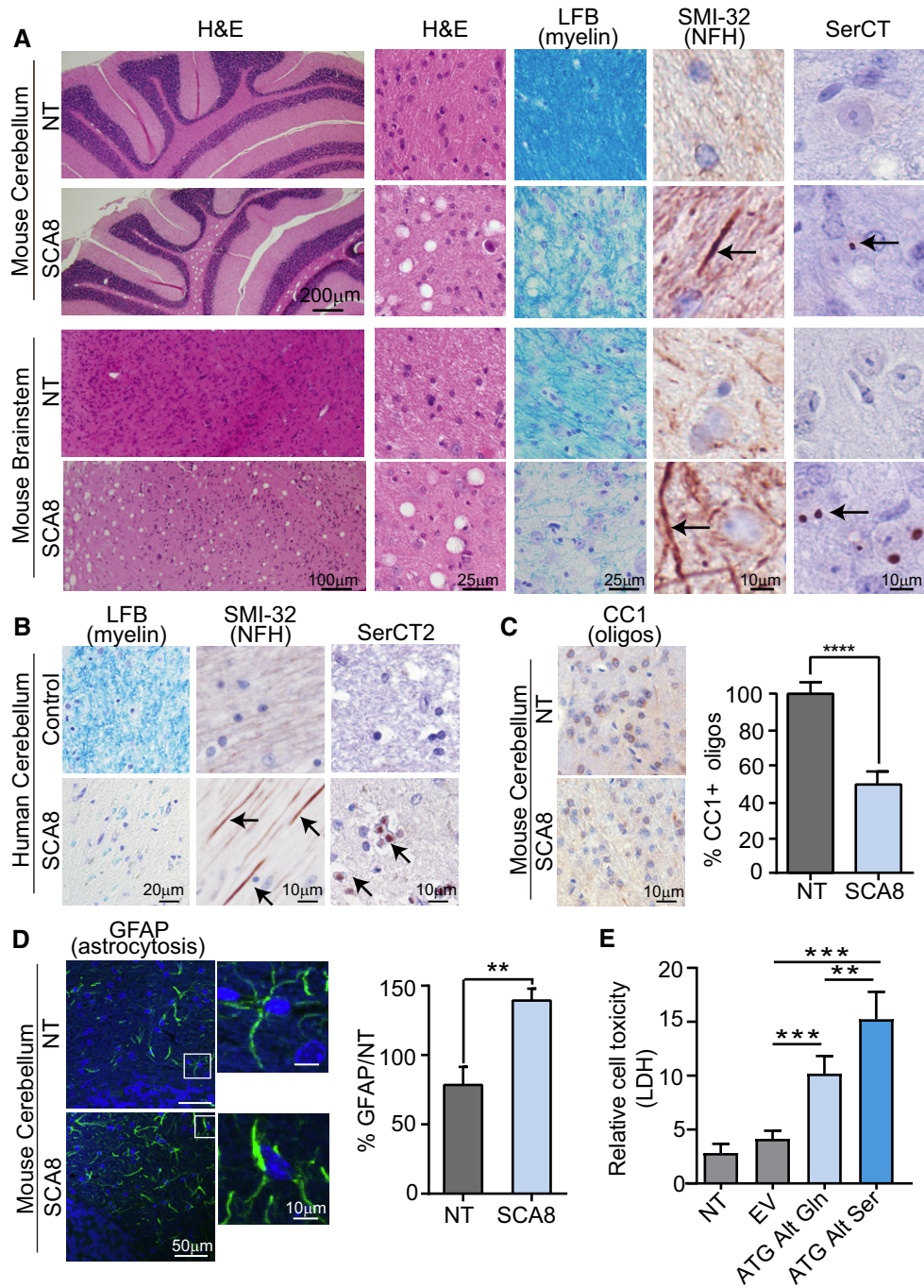
Figure 4. SCA8 BAC mice and human autopsy tissue show white matter abnormalities at sites of polySer accumulation.

A   Disease-specific sensitivity to vacuolization after prolonged storage in ethanol shown by H&E in cerebellar white matter and brainstem of 10- to 12-month-old end-stage SCA8 BAC mice but not in age-matched NT controls (n = 3) (panels 1&2). Demyelination shown by luxol fast blue staining (LFB) (panel 3) and axonal degeneration shown by α-SMI-32 (panel 4; degenerated axons are indicated by black arrows) observed in sites of polySer accumulation shown by α-SerCT (panel 5; representative aggregates are indicated by black arrows) in deep cerebellar white matter and brainstem in SCA8 BAC mice (lower panels) but not in NT mice (upper panels) (n = 3).

B   Demyelination shown by luxol fast blue staining (LFB) (panel 1) and axonal degeneration shown by α-SMI-32 (panel 2) observed sites of polySer accumulation shown by α-SerCT2 (panel 3) in deep cerebellar white matter was found in SCA8 autopsy tissue but not in control brains (n = 3).

C   Immunohistochemistry using CC1 (α-APC) antibody shows significantly lower numbers of mature oligodendrocytes in SCA8 BAC mice compared to NT mice (NT n = 5, SCA8 BAC n = 5; **** P < 0.0001; mean ± SEM; unpaired t-test).

D   Immunofluorescence using α-GFAP antibody shows significant increase in astrogliosis in SCA8 BAC mice compared to NT mice (NT n = 3, SCA8 BAC n = 3, **P < 0.01; mean ± SEM; unpaired t-test).

E   Cell death measured by lactase dehydrogenase (LDH) assay in T98 cells transfected with codon replacement constructs expressing polyGln (light blue) or polySer (dark blue). NT, nontransfected; EV, empty vector (n = 5, **P < 0.003; ***P < 0.0003; mean ± SEM; unpaired t-test).
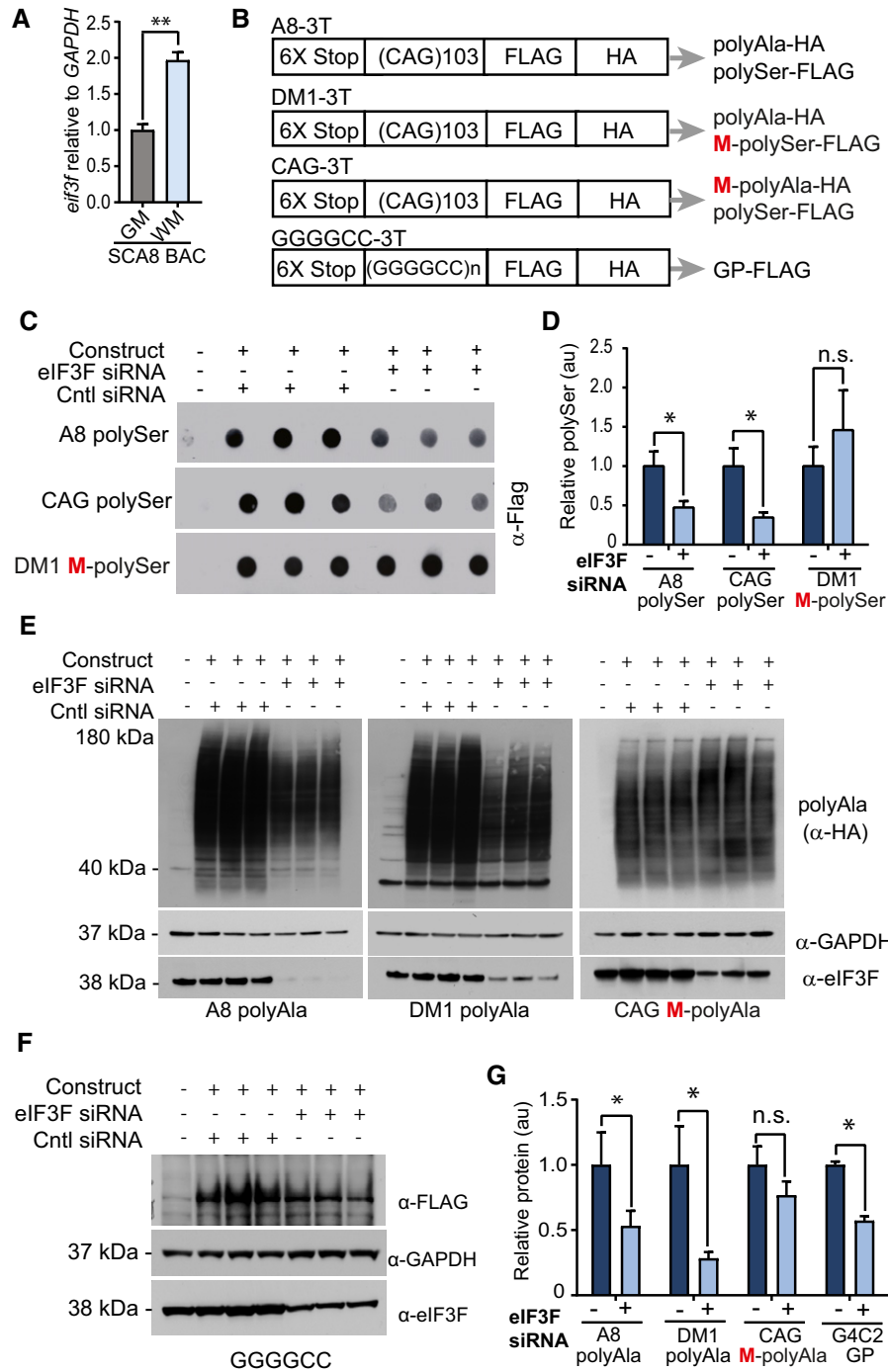
Figure 5.   Mammalian translation factor eIF3F is upregulated in symptomatic SCA8 BAC mice and can regulate RAN translation.

A   qRT–PCR showing *Eif3f* expression levels are increased twofold in SCA8 cerebellar white matter compared to SCA8 cerebellar gray matter (*n* = 3, **P < 0.01; mean ± SEM; unpaired *t*-test).

B   Schematic diagram showing constructs used for eIF3F knockdown experiments. All constructs have a tag in each reading frame. Red M indicates methionine (ATG) initiated reading frames.

C   Dot blot detection of polySer expression in using α-FLAG antibody showing decrease in RAN polySer but not ATG-polySer when HEK293 cells are co-transfected with eIF3F siRNA.

D   Quantification of polySer detection (*n* = 5, *P < 0.01; n.s. no significance; mean ± SEM; unpaired *t*-test).

E   Detection of polyAla expression using α-HA antibody showing decrease in RAN polyAla but not ATG-polyAla when HEK293 cells are co-transfected with eIF3F siRNA.

F   Detection of polyGP expression using α-FLAG antibody showing a decrease in RAN polyGP when HEK293 cells are co-transfected with eIF3F siRNA.

G   Quantification of polyAla and polyGP detection (*n* = 5, *P < 0.01; n.s. no significance; mean ± SEM; unpaired *t*-test).

Source data are available online for this figure.

Similarly, eIF3F knockdown in cells expressing constructs without an ATG-initiation codon in the polyAla reading frame (A8 and DM1) decreased steady-state levels of polyAla RAN proteins by 47% ($P < 0.05$) and 72% ($P < 0.05$), respectively. Similar to the polySer results, eIF3F knockdown in the presence of an ATG-initiation codon (CAG-3T) did not decrease polyAla accumulation (Fig 5E and G). In summary, these data show eIF3F modulates steady-state levels of RAN, but not ATG-initiated polySer and polyAla proteins.

Next, we tested whether eIF3F also affects RAN proteins expressed from the ALS/FTD causing GGGGCC repeats. Protein levels of glycine–proline (GP) from a GGGGCC expansion construct were measured by protein blotting. Similar to the results with the CAG expansion, eIF3F knockdown decreased levels of GP by 43% ($P < 0.05$; Fig 5F and G). Quantitative RT–PCR showed that eIF3F knockdown did not affect the levels of mRNA expressed from any of the minigene constructs (Fig EV4B).

Taken together, these data show that eIF3F knockdown can reduce steady-state levels of RAN proteins in multiple reading frames and across CAG and G4C2 repeat motifs.

Discussion

Here, we describe a novel CAG-encoded polySer RAN protein and provide evidence that it contributes to SCA8 pathology. First, we show SCA8 RAN polySer is found in affected brain regions of mouse and human autopsy tissue, including the cerebellum and brainstem. Second, although both proteins are expressed from CAG expansion transcripts, the SCA8 RAN polySer shows a distinct distribution pattern in the white matter compared to the previously described ATG-initiated polyGln protein, which accumulates in neurons. Third, SCA8 polySer RAN protein accumulation increases with age and disease progression in SCA8 BAC expansion mice. Fourth, white matter regions with RAN polySer staining show demyelination, axonal degeneration, and astrogliosis suggesting a role for SCA8 polySer RAN in neurodegeneration by loss of white matter integrity. Finally, we found that eiF3F, a mammalian translation factor, is expressed at higher levels in cerebellar white matter compared to gray matter. Interestingly, in vitro knockdown of eIF3F reduces RAN but not AUG-initiated expansion proteins, suggesting eIF3F may underlie the white matter-specific RAN protein accumulation now observed in several repeat expansion diseases (SCA8, DM2 and HD).

In addition to our current report of polySer, we previously reported the accumulation of RNA foci, polyAla, and polyGln proteins in SCA8 BAC mice and patient autopsy tissue. Initially, it was demonstrated that polyGln accumulates in Purkinje and pontine neuronal nuclei (Moseley et al, 2006). The present work extends the molecular characterization of SCA8 by showing polyGln aggregates are also found in the frontal cortex, pons, and hippocampus (Fig 2B), and are consistently located in neuronal nuclei (Fig 2C). RAN polyAla staining was previously reported in Purkinje cell soma and dendritic processes (Zu et al, 2011), and CUG RNA foci were detected in Purkinje cells, molecular layer interneurons, and Bergmann glia (Daughters et al, 2009). Additional studies are needed to investigate the brain distribution of polyAla and possible antisense RAN proteins.

Here, we provide the first in vivo evidence of a novel RAN polySer protein, which accumulates in white matter regions. This led to the discovery that SCA8 mice have widespread white matter abnormalities, which are first found in the cerebellum and brainstem. White matter degeneration phenotypes found in severely affected SCA8 mice raises the possibility that SCA8 initially involves myelin loss and axonal degeneration followed by loss of Purkinje cells and other neurons. Consistent with this hypothesis, sensory symptoms, including proprioception deficits indicative of polyneuropathy in patients, suggest neuronal loss in SCA8 may be triggered by a distal to proximal dying-back axonopathy (Gupta & Jankovic, 2009). It is also possible that the white matter abnormalities seen in SCA8 mice are early neurodegenerative features of the disease and that RAN protein accumulation in white matter regions triggers these abnormalities. At later stages of disease in the SCA8 mice and human autopsy tissue, RAN polySer aggregates are also found throughout the frontal cortex and hippocampus, a finding consistent with cognitive abnormalities in SCA8 patients (Juvonen et al, 2000; Stone et al, 2001; Zeman et al, 2004; Baba et al, 2005).

Similar to SCA8, RAN protein accumulation in white matter regions and white matter abnormalities have also been reported in HD (Bohanna et al, 2011; Bañez-Coronel et al, 2015) and DM2 (Ogata et al, 1998; Minnerop et al, 2011; Zu et al, 2017). Whether glial cells express RAN proteins or they respond to degeneration of neuronal processes is not clear. In HD, glial-specific expression of the expansion mutation results in the development of neurodegenerative phenotypes, highlighting the role of glia in disease (Huang et al, 2015). This model and additional animal models that selectively express expansion mutations in glial cells will be important for understanding the effects of RAN proteins on glia in repeat expansion diseases.

The greater level of SCA8 polySer toxicity compared to polyGln that we see in cell culture is consistent with previous findings in HD (Bañez-Coronel et al, 2015). The high toxicity of these homopolymeric polySer proteins suggests that they contribute to the white matter abnormalities found in the polySer-positive regions in both SCA8 and HD. The toxicity of SCA8 and HD polySer expansion proteins may be related to the propensity of these residues for post-translational modifications. For example, phosphorylation of serine residues in the microtubule-associated protein tau (MAPT) and TAR DNA binding proteins (TDP-43) causes toxic protein GOF effects in several neurodegenerative diseases (Sreedharan et al, 2008; Golde et al, 2010). Given the fact that bidirectional expression and RAN translation are found in a growing number of diseases, it is possible that polySer toxicity could also play a role in other CAG/CTG repeat expansion disorders including SCA1, SCA2, SCA3, SCA6, SCA12, SCA17, SBMA, DRPLA, and DM1.

Protein translation machinery in eukaryotes is well conserved; however, the components of this machinery vary between cell types and developmental stages (Sauert et al, 2015). The preferential accumulation of SCA8 RAN polySer and several other RAN proteins in white matter regions (Bañez-Coronel et al, 2015; Zu et al, 2017) suggests that RAN translation may be favored by one or more translation factors expressed in white matter. In vanishing white matter disease, mutations in the eukaryotic translation initiation factor eIF2B cause selective effects on glial cells (van der Knaap et al, 2006). Here, we demonstrate that reducing the levels of the mammalian eukaryotic translation initiation factor eIF3F decreases steady-state levels of several RAN but not AUG-initiated expansion proteins in cell culture.

Taken together, these data support a model in which protein translation from reading frames containing upstream AUG start codons initiates using met-tRNA$^{i}_{met}$ and the canonical protein translational machinery. In contrast, RAN translation which does not require an AUG start codon is sensitive to eIF3F levels. The AUG codon present in the polyGln reading frame could therefore explain the cell-type distribution difference between AUG-initiated polyGln and RAN proteins in both SCA8 and HD.

Because regulation of translation initiation plays a critical role in cellular homeostasis, global effects of any therapeutic perturbation on translation initiation machinery will need to be assessed carefully. While our results suggest that eIF3F plays a role in RAN translation and may be a therapeutic target for multiple microsatellite expansion disorders, it will be important to determine the potential risks and benefits of reduced eIF3F activity in brain. Additionally, more studies are required to understand the mechanism by which eIF3F regulates RAN translation.

The mammalian eIF3 complex is the largest initiation complex compromising 13 non-identical subunits (Hinnebusch, 2006). Among these, five "core" subunits (eIF3a, eIF3b, eIF3c, eIF3g, eIF3i) are conserved in yeast translation machinery and have also been shown to be sufficient for translation of mammalian transcripts (Naranda *et al*, 1994; Hinnebusch, 2006). The remaining "noncore" subunits including eIF3f appear to play a regulatory role in canonical and IRES translation initiation (Hashem *et al*, 2013; Cate, 2017). Consistent with a non-essential role for eIF3F, a gene-trap screen in two human cell lines identified a number of eIF3 subunit genes (*eIF3A, eIF3B, eIF3D, eIF3I, eIF3J, eIF3M*) but not *eIF3F* as important for optimal fitness (Blomen *et al*, 2015). While the specific functions of eIF3F are not well understood, the loss of *eIF3F* has been reported to contribute to tumorigenesis (Shi *et al*, 2006) and to induce muscle atrophy (Csibi *et al*, 2008). It has also been reported that the eIF3 complex binds to structured 5′ UTRs and recruits mRNAs directly to ribosomes independent of canonical scanning machinery (Lee *et al*, 2015). In our cell culture experiments, eIF3F knockdown was sufficient to decrease steady-state levels of RAN polySer and RAN polyAla, but did not reduce levels of ATG-initiated polySer or ATG-initiated polyAla proteins suggesting eIF3F may preferentially affect RAN proteins and could provide an opportunity to target RAN translation without interfering with canonical translation. Future studies in animal models and the generation and characterization of eIf3f knockout mice will be important to determine whether eIF3F/eIf3f knockdown can selectively reduce RAN protein accumulation without deleterious effects on protein homeostasis. Additional studies are also needed to understand how eIF3F affects RAN translation and whether these effects are direct or indirect.

In summary, we provide compelling evidence for the accumulation of a novel, toxic SCA8 polySer RAN protein that forms aggregates, which increase with age and disease severity. These polySer aggregates preferentially accumulate in WM regions that show demyelination and axonal degeneration. Additionally, we identify eIF3F as a translation initiation factor that selectively regulates RAN but not canonical translation and provides a novel entry point into identifying the RAN translation machinery.

Materials and Methods

DNA constructs and siRNAs

The FLAG-polySerCT construct was generated by subcloning *ATNX8* genomic sequence containing a CAG expansion of 82 repeats with 188 bp of downstream sequence into p3X FLAG-myc-CMV-24 vector (Sigma, St. Louis, MO) in the CAG direction. The genomic DNA used to generate this clone was amplified by PCR using genomic DNA from the SCA8 BAC expansion mice (2,878) and using a 5′ primer (5′ AGC TGA AGC TTG TTA AAA GAA GAT AAT ATA TTT AAA AAA TGC AG 3′) containing an added HindIII restriction enzyme site and the 3′ primer (5′ AGT CTG AAT TCC CTA GTT CTT GGC TCC AGA CTA AC 3′) containing an added EcoRI restriction enzyme site. The 5′ primer also contains a T/G base substitution to avoid the insertion of a stop codon in AGC reading frame between N-terminal FLAG and the repeat tract. The PCR product was cut with HindIII/EcoRI and cloned into p3X FLAG-myc-CMV-24 cut with the same enzymes. The presence of the N-terminal FLAG epitope tag in the polySer (AGC) frame, 82 CAG repeats, and 3′ flanking region spanning the first stop codon within polySer frame was confirmed by Sanger sequencing.

ATG-3T, A8-3T, DM1-3T, and GGGGCC-3T were previously generated and described (Zu *et al*, 2011, 2013).

siRNA targeting human eIF3F and a control non-targeting siRNA were ordered from GE Dharmacon (Lafayette, CO; control siRNA: D-002810-01-05, eIF3F:J-019535-10).

To assess toxicity of individual RAN proteins, ATG-initiated non-hairpin forming alternative codon minigenes were generated and synthesized by IDT Technologies and subcloned into pcDNA3.1-3T vector in frame with the 3′ FLAG tag. PolyGln is encoded by CAA repeats, and polySer is encoded by TCT-TCC. To better imitate the SCA8 RAN proteins, the C-terminal region of the polySer protein is included after the polyprotein stretch. The polyGln protein is directly followed by several stop codons, therefore, polyGln does not have a unique C-terminal sequence.

Cell culture and transfections

HEK293T cells, which express high levels of RAN proteins (Zu *et al*, 2011), were cultured in DMEM supplemented with 10% fetal bovine serum (FBS) and incubated at 37°C in a humid atmosphere containing 5% CO_2. Plasmid and siRNA transfections were done with Lipofectamine 2000 (Invitrogen, Carlsbad, CA) according to manufacturer's instructions. Cells were collected 48 h post-transfection for subsequent analysis. For KD experiments, HEK293T cells were transfected with 30 nM siRNA using Lipofectamine 2000. Twenty-four hours post-transfection, repeat containing plasmid and 30 nM siRNA were co-transfected. Cells were collected 48 h after the first second round of transfection.

LDH cytotoxicity assay

Cell toxicity was measured in T98 cells and assessed by measuring lactate dehydrogenase (LDH) released into the medium by dying cells (CytoTox 96 Nonradioactive Cytotoxicity Assay, Promega, Madison, WI) following the manufacturer's protocol. Absorbance was recorded at 490 nm, and total LDH release was measured by

lysing the cells with 1% Triton X-100. LDH determinants were measured in three independent experiments and each experiment performed in quintuplicates for each condition (Korzeniewski & Callewaert, 1983).

Real-time quantitative PCR

Quantification of transcript levels in cells transiently transfected with triple-tagged constructs was performed using the 5′FLAG (5′ GAT TAC AAG GAC GAC GAC GAC 3′) and 3′HIS (5′ ATG GTC ATG GTG ATG ATG ACC 3′) primers. Control reactions were performed using human β-actin forward (5′ TCG TGC GTG ACA TTA AGG AG 3′) and human β-actin reverse (5′ GAT CTT CAT TGT GCT GGG TG 3′) primers.

eIF3F and MBP in white matter vs. gray matter were measured using Bio-Rad PrimePCR SYBR Green Assay primers (Bio-Rad, Hercules, CA). Detection of ATXN8 in SCA8 BAC mouse was previously described in Moseley et al, 2006.

Production of rabbit polyclonal antibodies

The polyclonal rabbit antibodies against polySer RAN protein were generated by New England Peptide (NEP, Gardner, MA). Rabbit antisera were raised against synthetic peptides Ac-CRVNLSVEAGSQKRQSE-amide and Ac-CSSSKARFSNMKD-amide for α-SerCT (NEP, Project #1306, Rabbit #F3672) and α-SerCT2 (NEP, Project #2953, Rabbit #I2108), respectively.

Human autopsy tissue

Control and SCA8 autopsy tissue were collected at the University of Minnesota and the University of Florida with informed consent of patients or their relatives and approval of respective institutional review boards.

Mouse samples

Mice used in this study were housed and treated in accordance with the NIH Guide for the Care and Use of Laboratory Animals. All animal studies were approved by Animal Care and Use Committee at the University of Florida. Previously described SCA8 BAC transgenic lines on the FVB background (BAC EXP2, 2878) were used (Moseley et al, 2006). Hemizygous mice with the SCA8 BAC transgene were by genotyped by PCR as previously described (Moseley et al, 2006). Due to severe motor dysfunction that SCA8 BAC expansion mice exhibit after 5 months of age, additional food (GelDiet, Clear H_2O, Westbrook, MA) was provided in the bottom of the cage for animals > 5 months. For histological analysis, animals were anesthetized using 100 mg of ketamine and 20 mg of xylazine per kg of body weight and perfused through the ascending aorta with 15 ml of isotonic saline, followed by 10 ml of 10% buffered formalin. For total RNA isolation, mice were euthanized by CO_2 inhalation followed by cervical dislocation.

Gait analysis

Digital video images of the mouse paws were collected with a high-speed video camera set up beneath the transparent belt of a motorized treadmill (DigiGait™ Imaging system, Mouse Specifics, Framingham, MA). SCA8 BAC mice and their littermates were tested at 2 months of age. Each mouse was allowed to explore the tread-mill and habituate to the task for 1 min with the motor speed set to 12 cm/s. Motor speed was increased to 22 cm/s for data collection. Approximately 5-s of video recording in which the mouse walked straight ahead in a constant relative position with respect to the camera was used for analysis. Data from each paw were analyzed with DigiGait automated gait analysis software, and the 45 parameters measured by the software are outlined in Table 2 (Mouse Specifics).

Open field analysis

Open field analysis was performed by testing mouse behavior during a 30-min session in a completely dark 17″ × 17″ open chamber (Med Associates, Inc., Fairfax, VT). Mice were allowed to acclimate to the testing room for approximately 2 h before the start of analysis. Mice were then placed in the center of the darkened activity-monitoring chamber. Data were analyzed with Activity Monitor software (Med Associates, Inc.; Bolivar et al, 2000).

Immunofluorescence

Polyclonal rabbit antibodies were tested in vitro for their specificity to recombinant SCA8 polySer RAN. HEK293T cells were cultured on coverslips in six-well tissue-culture plates and transfected with the FLAG-polySerCT plasmid the next day. Forty-eight hours post-transfection, cells were fixed in 4% paraformaldehyde in PBS for 20 min and permeabilized in 0.5% Triton X-100 in PBS for 10 min on ice. The coverslips were blocked in 1% normal goat serum (NGS) in PBS for 30 min. After blocking, the cells were incubated for 1 h at room temperature in blocking solution containing the α-FLAG (1:200; A8592, Sigma) primary antibodies and α-SerCT polyclonal antibodies (1:1,000). The coverslips were washed three times in PBS and incubated for 1 h at 37°C in blocking solution containing secondary antibodies. Goat α-mouse conjugated to Cy3 (Jackson ImmunoResearch, West Grove, PA) and goat α-rabbit conjugated to Alexa Fluor 488 (Invitrogen) were used at a dilution of 1:200. Slides were washed three times for 5 min in 1× PBS, mounted with Prolong Diamond Antifade Mounting Medium with DAPI (Invitrogen), and coverslipped. Mouse α-NeuN antibody (ABN78A4, Millipore Sigma, Burlington, MA) was used for co-staining with custom rabbit polyclonal α-SerCT antibody, and rabbit α-NeuN antibody (ab104225, Abcam, Cambridge, MA) was used for co-staining with mouse 1C2 antibody (MAB1574, Millipore Sigma).

Immunofluorescence using α-GFAP or α-CNPase was performed on fixed mouse brain sections. The sections were deparaffinized in xylene and rehydrated through an alcohol gradient. Heat-induced antigen retrieval was performed in 10 mM citrate buffer (pH = 6.0). Non-specific binding was blocked using 2% FBS solution in 1× PBS. Rabbit polyclonal α-GFAP antibody (1:1,000; Biogenex, Fremont, CA) and α-CNPase (1:200; ab6319, Abcam) were applied at 4°C overnight. The sections were washed three times in 1× PBS, and α-rabbit antibody conjugated to Alexa Fluor 488 (Invitrogen) was used at a dilution of 1:200. Slides were washed three times for 5 min in 1× PBS, mounted with Prolong Diamond Antifade Mounting Medium with DAPI (Invitrogen), and coverslipped. Images were

taken with a Leica confocal microscope (Leica Microsystems, Wetzlar, Germany).

Histology and immunohistochemistry

For the detection of polySer RAN proteins using the C-terminal antibodies and the fresh-frozen mouse brain tissue, the following protocol was used. Brains were collected and frozen in 2-methylbutane cooled with liquid nitrogen. Seven-micrometer sagittal sections were cut using cryostat and fixed in 10% buffered formalin for 15 min. Endogenous peroxidase block was performed in 3% H_2O_2 methanol for 5 min. To block non-specific binding a non-serum block (Biocare Medical, Pacheco, CA) was applied for 15 min. Primary antisera were applied in 1:10 non-serum block at 4°C overnight at the following dilutions; α-SerCT (1:10,000), α-SerCT2 (1:5,000), or corresponding preimmune sera at the same dilutions. The sections were washed three times in 1× PBS and biotin-labeled rabbit secondary antibody (Biolegend, San Diego, CA) applied at room temperature for 30 min. A horseradish peroxidase-conjugated linking reagent (Biolegend) was applied for 30 min at room temperature, and detection was performed by exposure to vector nova red substrate kit (Vector Laboratories, Inc., Burlingame, CA). For counterstaining, hematoxylin solution (Vector Laboratories, Inc.) was applied for 20-s. Slides were dehydrated in graded ethanol and xylene solutions and mounted using CytoSeal 60 (Electron Microscopy Sciences, Hatfield, PA).

For detection of polySer RAN protein in fixed brain tissue, animals were perfused transcardially with 1× PBS and 10% buffered formalin. Brains were collected and stored in 10% formalin for 24 h and later removed into 70% ethanol. After histological processing and paraffin embedding, seven-micrometer sagittal sections were cut using a microtome. Sections were deparaffinized in xylene (15 min two times) and rehydrated through an alcohol gradient (10 min at each step). Sections were then treated with the following antigen retrieval steps: first, 1 μg/ml proteinase K treatment in 1 mM $CaCl_2$, 50 mM Tris buffer (pH = 7.6) for 30 min at 37°C; second, pressure cooked in 10 mM EDTA (pH = 6.5) for 15 min using microwave as a heat source; and third, 95% formic acid treatment for 5 min (Kai *et al*, 2012). Endogenous peroxidase was blocked in 3% H_2O_2 methanol for 10 min. To block non-specific binding, a non-serum block (Biocare Medical, Pacheco, CA) was applied for 15 min. Primary antisera were applied in 1:10 non-serum block at 4°C overnight with α-SerCT (1:10,000), α-SerCT2 (1:5,000), or corresponding preimmune sera in the same concentrations. The sections were washed three times in 1× PBS and biotin-labeled rabbit secondary antibody (Biolegend) applied at room temperature for 30 min. A horseradish peroxidase-conjugated linking reagent was applied for 30 min at room temperature and detection was performed by exposure to the Vector Red Substrate Kit (Vector Laboratories, Inc.). Hematoxylin solution was applied for 20-s (Vector Laboratories, Inc.).

Immunostaining experiments using α-APC CC1 (1:1,000; Calbiochem, San Diego, CA), α-SMI-32 (1:3,000; Covance, Princeton, NJ), and α-FLAG (1:1,000; Sigma) antibodies were performed in similar way as above except that a milder heat-induced antigen retrieval was performed in 10 mM citrate buffer (pH = 6.0) using a steamer instead of pressure cooker. For hematoxylin and eosin staining, seven micron mouse and human brain sections were deparaffinized

in xylene and dehydrated through graded ethanol. The slides were then soaked in hematoxylin (Sigma) for 1 min and washed in running distilled water for 10 min. Next, the slides were immersed in Eosin Y (Sigma) for 30 s and washed in distilled water for 10 min. The slides were rehydrated and coverslipped before visualization.

For luxol fast blue (LFB) staining, 7 μm mouse and human brain sections were deparaffinized in xylene and hydrated to 95% ethyl alcohol. The sections were left in LFB solution (0.1% luxol fast blue in 95% ethyl alcohol) at 56°C overnight. The next day, slides were rinsed in 95% ethyl alcohol and distilled water. Subsequently, the slides were differentiated in the lithium carbonate solution and 70% ethyl alcohol (30 s, each) and washed in distilled water. The slides were counterstained in the cresyl violet solution (0.1% cresyl violet in distilled water) for 40 s, rinsed in distilled water. The slides were rehydrated and coverslipped before visualization. Images were captured with an Olympus BX51 light microscope.

Statistical analysis

Statistical significance was assessed by the unpaired Student's *t*-test. LDH toxicity assays were corrected for multiple comparisons. Statistics were performed using the software package Prism 5 (GraphPad Software Inc, GraphPad Software, Inc., La Jolla, CA).

Protein blotting

Cells were lysed with RIPA (150 mM NaC1, 1% sodium deoxycholate, 1% Triton X-100, 50 mM Tris–HCl; pH = 7.5) buffer with proteinase inhibitors (Roche) at 4°C with shaking for 30 min. Genomic DNA was sheared with a 21-gauge needle, and lysates were centrifuged at 4°C at 15,000 *g* for 15 min. Protein in the soluble fraction of the lysates was quantified by Bradford assay (Bio-Rad, Hercules, CA). Lysates were run 4–12% Bis-Tris gel (Bio-Rad) and transferred to nitrocellulose membrane. Membranes were blotted with the antibodies at 4°C shaking overnight: α-FLAG-HRP (1:3,000; Sigma), α-HA (1:2,000; Sigma), α-GAPDH (1:10,000, Millipore, Burlington, MA), α-polySer1 (1:10,000, custom antibody) in 1% milk in phosphate-buffered saline with Tween 20 (PBST). Membranes were washed in PBST for 5 min three times and incubated in secondary antibody solutions conjugated to horseradish peroxidase (1:2,500; GE Healthcare, Lafayette, CO) for 45 min at room temperature. Membranes were washed again in PBST and developed with the application of the substrate for enhanced chemiluminescence (ECL) for 1 min (PerkinElmer, Waltham, MA).

Insoluble pellets were resuspended in 2% SDS and incubated at 65°C. Resulting SDS soluble fraction was immobilized onto nitrocellulose membranes with Bio-Dot 96-well microfiltration system (Bio-Rad) under vacuum. The membranes were washed with PBST and blotted using the same protocol as Western blotting.

RNA isolation

Whole cerebellum was removed, cut into pieces, and lysed in TRI reagent (Invitrogen). Total RNA was isolated using chloroform extraction and precipitated using isopropanol. The RNA pellet was washed with 70% ethanol in DEPC water and dissolved in 30 μl of DEPC water. Any contaminant genomic DNA was removed using

Turbo DNase I (Thermo Fisher, Waltham, MA). RNA quantification was performed using Nanodrop and Quant-iT™ Ribogreen RNA Assay Kits (Thermo Fisher).

High-throughput cDNA sequencing

The integrity of RNA samples obtained from three SCA8 BAC expansion and three non-transgenic control mice was assessed using 2100 Bioanalyzer (Agilent, Santa Clara, CA), and samples with RNA integrity number (RIN) > 8 were used for further analysis. Single-stranded cDNA libraries were prepared at New York Genome Centre (NYGC, New York, NY). The libraries were sequenced using Illumina Hiseq2500 platform generating paired reads of 125 bp.

RNA-Seq analysis

To compare expression levels of *ATXN8* and *ATXN8OS*, the human reference sequence containing *ATXN8OS* and 10 kb upstream and downstream sequence was indexed using HiSat2 (Kim *et al*, 2015). This indexed sequence was then used as the reference genome, and raw reads generated by RNA-Seq were fed into HiSat2 aligner. The resulting alignments to the *ATXN8/ATXN8OS* locus were visualized by Integrated Genomic Viewer (Robinson *et al*, 2011). Fragment per kilobase million (FPKM) of *ATXN8* and *ATXN8OS* was calculated by normalizing the read count mapped to gene-specific regions of ATXN8 and ATXN8OS to the length. The difference was calculated by dividing both FPKM values by *ATXN8OS* FPKM value. This analysis was done on three biological replicates, and statistical significance was calculated using an unpaired *t*-test.

Expanded View for this article is available online.

Author contributions
FA and LPWR conceived the project. FA, BAP, HKS, MB-C, and TZ conducted experiments. FA, BAP, TZ, ETW, ATY, HKS, and MB-C analyzed data. HF, HBC, JCT, CAR, SHS, TA, TR, and LPWR provided human autopsy tissue. FA, BAP, and LPWR wrote the manuscript. All authors discussed the results and commented on the manuscript.

Conflict of interest
F.A., T.Z., and L.P.W.R. have patents pending on RAN translation.

References

Ash PE, Bieniek KF, Gendron TF, Caulfield T, Lin WL, Dejesus-Hernandez M, van Blitterswijk MM, Jansen-West K, Paul JW III, Rademakers R, Boylan KB, Dickson DW, Petrucelli L (2013) Unconventional translation of C9ORF72 GGGGCC expansion generates insoluble polypeptides specific to c9FTD/ALS. *Neuron* 77: 639–646

Baba Y, Uitti RJ, Farrer MJ, Wszolek ZK (2005) Sporadic SCA8 mutation resembling corticobasal degeneration. *Parkinsonism Relat Disord* 11: 147–150

Bañez-Coronel M, Ayhan F, Tarabochia AD, Zu T, Perez BA, Tusi SK, Pletnikova O, Borchelt DR, Ross CA, Margolis RL, Yachnis AT, Troncoso JC, Ranum LP (2015) RAN translation in Huntington disease. *Neuron* 88: 667–677

Blomen VA, Májek P, Jae LT, Bigenzahn JW, Nieuwenhuis J, Staring J, Sacco R, van Diemen FR, Olk N, Stukalov A, Marceau C, Janssen H, Carette JE, Bennett KL, Colinge J, Superti-Furga G, Brummelkamp TR (2015) Gene essentiality and synthetic lethality in haploid human cells. *Science* 350: 1092–1096

Bohanna I, Georgiou-Karistianis N, Sritharan A, Asadi H, Johnston L, Churchyard A, Egan G (2011) Diffusion tensor imaging in Huntington's disease reveals distinct patterns of white matter degeneration associated with motor and cognitive deficits. *Brain Imaging Behav* 5: 171–180

Bolivar VJ, Caldarone BJ, Reilly AA, Flaherty L (2000) Habituation of activity in an open field: a survey of inbred strains and F1 hybrids. *Behav Genet* 30: 285–293

Cate JH (2017) Human eIF3: from 'blobology' to biological insight. *Philos Trans R Soc Lond B Biol Sci* 372: 20160176

Cognat E, Cleophax S, Domenga-Denier V, Joutel A (2014) Early white matter changes in CADASIL: evidence of segmental intramyelinic oedema in a pre-clinical mouse model. *Acta Neuropathol Commun* 2: 49

Csibi A, Tintignac LA, Leibovitch MP, Leibovitch SA (2008) eIF3-f function in skeletal muscles: to stand at the crossroads of atrophy and hypertrophy. *Cell Cycle* 7: 1698–1701

Daughters RS, Tuttle DL, Gao W, Ikeda Y, Moseley ML, Ebner TJ, Swanson MS, Ranum LP (2009) RNA gain-of-function in spinocerebellar ataxia type 8. *PLoS Genet* 5: e1000600

Day JW, Schut LJ, Moseley ML, Durand AC, Ranum LP (2000) Spinocerebellar ataxia type 8: clinical features in a large family. *Neurology* 55: 649–657

Felling RJ, Barron TF (2005) Early onset of ataxia in a child with a pathogenic SCA8 allele. *Pediatr Neurol* 33: 136–138

Garman RH (2011) Histology of the central nervous system. *Toxicol Pathol* 39: 22–35

Golde TE, Petrucelli L, Lewis J (2010) Targeting Abeta and tau in Alzheimer's disease, an early interim report. *Exp Neurol* 223: 252–266

Gupta A, Jankovic J (2009) Spinocerebellar ataxia 8: variable phenotype and unique pathogenesis. *Parkinsonism Relat Disord* 15: 621–626

Hashem Y, des Georges A, Dhote V, Langlois R, Liao HY, Grassucci RA, Pestova TV, Hellen CU, Frank J (2013) Hepatitis-C-virus-like internal ribosome entry sites displace eIF3 to gain access to the 40S subunit. *Nature* 503: 539–543.

Hinnebusch AG (2006) eIF3: a versatile scaffold for translation initiation complexes. *Trends Biochem Sci* 31: 553–562

Holcik M, Sonenberg N (2005) Translational control in stress and apoptosis. *Nat Rev Mol Cell Biol* 6: 318–327

Huang B, Wei W, Wang G, Gaertig MA, Feng Y, Wang W, Li X-J, Li S (2015) Mutant huntingtin downregulates myelin regulatory factor-mediated myelin gene expression and affects mature oligodendrocytes. *Neuron* 85: 1212–1226

Ishiguro T, Sato N, Ueyama M, Fujikake N, Sellier C, Kanegami A, Tokuda E, Zamiri B, Gall-Duncan T, Mirceta M, Furukawa Y, Yokota T, Wada K, Taylor JP, Pearson CE, Charlet-Berguerand N, Mizusawa H, Nagai Y, Ishikawa K (2017) Regulatory role of RNA chaperone TDP-43 for RNA misfolding and repeat-associated translation in SCA31. *Neuron* 94: 108–124 e107

Juvonen V, Hietala M, Päivärinta M, Rantamäki M, Hakamies L, Kaakkola S, Vierimaa O, Penttinen M, Savontaus ML (2000) Clinical and genetic

findings in Finnish ataxia patients with the spinocerebellar ataxia 8 repeat expansion. *Ann Neurol* 48: 354–361

Kai H, Shin R-W, Ogino K, Hatsuta H, Murayama S, Kitamoto T (2012) Enhanced antigen retrieval of amyloid β immunohistochemistry: re-evaluation of amyloid β pathology in Alzheimer disease and its mouse model. *J Histochem Cytochem* 60: 761–769

Kim JS, Son TO, Youn J, Ki CS, Cho JW (2013) Non-ataxic phenotypes of SCA8 mimicking amyotrophic lateral sclerosis and Parkinson disease. *J Clin Neurol* 9: 274–279

Kim D, Langmead B, Salzberg SL (2015) HISAT: a fast spliced aligner with low memory requirements. *Nat Methods* 12: 357–360

van der Knaap MS, Pronk JC, Scheper GC (2006) Vanishing white matter disease. *Lancet Neurol* 5: 413–423

Koob MD, Moseley ML, Schut LJ, Benzow KA, Bird TD, Day JW, Ranum LP (1999) An untranslated CTG expansion causes a novel form of spinocerebellar ataxia (SCA8). *Nat Genet* 21: 379–384

Korzeniewski C, Callewaert DM (1983) An enzyme-release assay for natural cytotoxicity. *J Immunol Methods* 64: 313–320

Kumar N, Miller GM (2008) White matter hyperintense lesions in genetically proven spinocerebellar ataxia 8. *Clin Neurol Neurosurg* 110: 65–68

Kuwamura M, Maeda M, Kuramoto T, Kitada K, Kanehara T, Moriyama M, Nakane Y, Yamate J, Ushijima T, Kotani T, Serikawa T (2002) The myelin vacuolation (mv) rat with a null mutation in the attractin gene. *Lab Invest* 82: 1279–1286

Lee ASY, Kranzusch PJ, Cate JHD (2015) eIF3 targets cell-proliferation messenger RNAs for translational activation or repression. *Nature* 522: 111–114

Lilja A, Hämäläinen P, Kaitaranta E, Rinne R (2005) Cognitive impairment in spinocerebellar ataxia type 8. *J Neurol Sci* 237: 31–38

Mills JD, Kavanagh T, Kim WS, Chen BJ, Kawahara Y, Halliday GM, Janitz M (2013) Unique transcriptome patterns of the white and grey matter corroborate structural and functional heterogeneity in the human frontal lobe. *PLoS One* 8: e78480

Minnerop M, Weber B, Schoene-Bake JC, Roeske S, Mirbach S, Anspach C, Schneider-Gold C, Betz RC, Helmstaedter C, Tittgemeyer M, Klockgether T, Kornblum C (2011) The brain in myotonic dystrophy 1 and 2: evidence for a predominant white matter disease. *Brain* 134: 3530–3546

Mori K, Weng SM, Arzberger T, May S, Rentzsch K, Kremmer E, Schmid B, Kretzschmar HA, Cruts M, Van Broeckhoven C, Haass C, Edbauer D (2013) The C9orf72 GGGGCC repeat is translated into aggregating dipeptide-repeat proteins in FTLD/ALS. *Science* 339: 1335–1338

Moseley ML, Zu T, Ikeda Y, Gao W, Mosemiller AK, Daughters RS, Chen G, Weatherspoon MR, Clark HB, Ebner TJ, Day JW, Ranum LP (2006) Bidirectional expression of CUG and CAG expansion transcripts and intranuclear polyglutamine inclusions in spinocerebellar ataxia type 8. *Nat Genet* 38: 758–769

Naranda T, MacMillan SE, Hershey JW (1994) Purified yeast translational initiation factor eIF-3 is an RNA-binding protein complex that contains the PRT1 protein. *J Biol Chem* 269: 32286–32292

Ogata A, Terae S, Fujita M, Tashiro K (1998) Anterior temporal white matter lesions in myotonic dystrophy with intellectual impairment: an MRI and neuropathological study. *Neuroradiology* 40: 411–415

Robinson JT, Thorvaldsdóttir H, Winckler W, Guttman M, Lander ES, Getz G, Mesirov JP (2011) Integrative genomics viewer. *Nat Biotechnol* 29: 24–26

Sauert M, Temmel H, Moll I (2015) Heterogeneity of the translational machinery: Variations on a common theme. *Biochimie* 114: 39–47

Schmahmann JD, Smith EE, Eichler FS, Filley CM (2008) Cerebral white matter: neuroanatomy, clinical neurology, and neurobehavioral correlates. *Ann N Y Acad Sci* 1142: 266–309

Shi J, Kahle A, Hershey JWB, Honchak BM, Warneke JA, Leong SPL, Nelson MA (2006) Decreased expression of eukaryotic initiation factor 3f deregulates translation and apoptosis in tumor cells. *Oncogene* 25: 4923–4936

Sreedharan J, Blair IP, Tripathi VB, Hu X, Vance C, Rogelj B, Ackerley S, Durnall JC, Williams KL, Buratti E, Baralle F, de Belleroche J, Mitchell JD, Leigh PN, Al-Chalabi A, Miller CC, Nicholson G, Shaw CE (2008) TDP-43 mutations in familial and sporadic amyotrophic lateral sclerosis. *Science* 319: 1668–1672

Stone J, Smith L, Watt K, Barron L, Zeman A (2001) Incoordinated thought and emotion in spinocerebellar ataxia type 8. *J Neurol* 248: 229–232

Todd PK, Oh SY, Krans A, He F, Sellier C, Frazer M, Renoux AJ, Chen KC, Scaglione KM, Basrur V, Elenitoba-Johnson K, Vonsattel JP, Louis ED, Sutton MA, Taylor JP, Mills RE, Charlet-Berguerand N, Paulson HL (2013) CGG repeat-associated translation mediates neurodegeneration in fragile X tremor ataxia syndrome. *Neuron* 78: 440–455

Wells GA, Wells M (1989) Neuropil vacuolation in brain: a reproducible histological processing artefact. *J Comp Pathol* 101: 355–362

Yokoyama T, Ishiyama M, Hasegawa K, Uchihara T, Yagishita S (2014) Novel neuronal cytoplasmic inclusions in a patient carrying SCA8 expansion mutation. *Neuropathology* 34: 27–31

Zeman A, Stone J, Porteous M, Burns E, Barron L, Warner J (2004) Spinocerebellar ataxia type 8 in Scotland: genetic and clinical features in seven unrelated cases and a review of published reports. *J Neurol Neurosurg Psychiatry* 75: 459–465

Zhou M, Sandercock AM, Fraser CS, Ridlova G, Stephens E, Schenauer MR, Yokoi-Fong T, Barsky D, Leary JA, Hershey JW, Doudna JA, Robinson CV (2008) Mass spectrometry reveals modularity and a complete subunit interaction map of the eukaryotic translation factor eIF3. *Proc Natl Acad Sci USA* 105: 18139–18144

Zu T, Gibbens B, Doty NS, Gomes-Pereira M, Huguet A, Stone MD, Margolis J, Peterson M, Markowski TW, Ingram MA, Nan Z, Forster C, Low WC, Schoser B, Somia NV, Clark HB, Schmechel S, Bitterman PB, Gourdon G, Swanson MS et al (2011) Non-ATG-initiated translation directed by microsatellite expansions. *Proc Natl Acad Sci USA* 108: 260–265

Zu T, Liu Y, Bañez-Coronel M, Reid T, Pletnikova O, Lewis J, Miller TM, Harms MB, Falchook AE, Subramony SH, Ostrow LW, Rothstein JD, Troncoso JC, Ranum LP (2013) RAN proteins and RNA foci from antisense transcripts in C9ORF72 ALS and frontotemporal dementia. *Proc Natl Acad Sci USA* 110: E4968–E4977

Zu T, Cleary JD, Liu Y, Bañez-Coronel M, Bubenik JL, Ayhan F, Ashizawa T, Xia G, Clark HB, Yachnis AT, Swanson MS, Ranum LPW (2017) RAN translation regulated by muscleblind proteins in myotonic dystrophy type 2. *Neuron* 95: 1292–1305 e1295